

Tracking of a Mobile Target Using Generalized Polarization Tensors*

Habib Ammari[†] Thomas Boulier[†] Josselin Garnier[‡] Hyeonbae Kang[§]
 Han Wang[†]

November 1, 2018

Abstract

In this paper we apply an extended Kalman filter to track both the location and the orientation of a mobile target from multistatic response measurements. We also analyze the effect of the limited-view aspect on the stability and the efficiency of our tracking approach. Our algorithm is based on the use of the generalized polarization tensors, which can be reconstructed from the multistatic response measurements by solving a linear system. The system has the remarkable property that low order generalized polarization tensors are not affected by the error caused by the instability of higher orders in the presence of measurement noise.

Mathematics Subject Classification (MSC2000): 35R30, 35B30

Keywords: generalized polarization tensors, target tracking, extended Kalman filter, position and orientation tracking, limited-view data, instability

1 Introduction

With each domain and material parameter, an infinite number of tensors, called the Generalized Polarization Tensors (GPTs), is associated. The concept of GPTs was introduced in [6, 4]. The GPTs contain significant information on the shape of the domain [3, 7, 9]. It occurs in several interesting contexts, in particular, in low-frequency scattering [15, 4], asymptotic models of dilute composites (see [23] and [10]), in invisibility cloaking in the quasi-static regime [8] and in potential theory related to certain questions arising in hydrodynamics [24].

Another important use of this concept is for imaging diametrically small conductivity inclusions from boundary or multistatic response measurements. Multistatic response

*This work was supported by ERC Advanced Grant Project MULTIMOD–267184 and NRF grants No. 2009-0090250 and 2010-0017532.

[†]Department of Mathematics and Applications, Ecole Normale Supérieure, 45 Rue d’Ulm, 75005 Paris, France (habib.ammari@ens.fr, boulier@dma.ens.fr, han.wang@ens.fr).

[‡]Laboratoire de Probabilités et Modèles Aléatoires & Laboratoire Jacques-Louis Lions, Université Paris VII, 75205 Paris Cedex 13, France (garnier@math.jussieu.fr).

[§]Department of Mathematics, Inha University, Incheon 402-751, Korea (hbkang@inha.ac.kr).

measurements are obtained using arrays of point source transmitters and receivers. This measurement configuration gives the so-called multistatic response matrix (MSR), which measures the change in potential field due to a conductivity inclusion. In fact, the GPTs are the basic building blocks for the asymptotic expansions of the perturbations of the MSR matrix due to the presence of small conductivity inclusions inside a conductor [17, 12, 6]. They can be reconstructed from the multi-static response (MSR) matrix by solving a linear system. The system has the remarkable property that low order generalized polarization tensors are not affected by the error caused by the instability of higher orders in the presence of measurement noise. Based on the asymptotic expansion, efficient and direct (non-iterative) algorithms to determine the location and some geometric features of the inclusions were proposed. We refer to [4, 5] and the references therein for recent developments of this theory. An efficient numerical code for computing the GPTs is described in [11].

In [2], we have analyzed the stability and the resolving order of GPT in a circular full angle of view setting with coincident sources and receivers, and developed efficient algorithms for target identification from a dictionary by matching the contracted GPTs (CGPTs). The CGPTs are particular linear combinations of the GPTs (called harmonic combinations) and were first introduced in [8]. As a consequence, explicit relations between the CGPT of scaled, rotated and translated objects have been established in [2], which suggest strongly that the GPTs can also be used for tracking the location and the orientation of a mobile object. One should have in mind that, in real applications, one would like to localize the target and reconstruct its orientation directly from the MSR data without reconstructing the GPTs.

In this paper we apply an extended Kalman filter to track both the location and the orientation of a mobile target directly from MSR measurements.

The Extended Kalman Filter (EKF) is a generalization of the Kalman Filter (KF) to nonlinear dynamical systems. It is robust with respect to noise and computationally inexpensive, therefore is well suited for real-time applications such as tracking [26].

Target tracking is an important task in sonar and radar imaging, security technologies, autonomous vehicle, robotics, and bio-robotics, see, for instance, [13, 14, 16, 18, 19, 25]. An example in bio-robotics is the weakly electric fish which has the faculty to probe an exterior target with its electric dipole and multiple sensors distributed on the skin [1]. The fish usually swims around the target to acquire information. The use of Kalman-type filtering for target tracking is quite standard, see, for instance, [13, 14, 16, 18, 19, 25].

However, to the best of our knowledge, this is the first time where tracking of the orientation of a target is provided. Moreover, we analyze the ill-posed character of both the location and orientation tracking in the case of limited-view data. In practice, it is quite realistic to have the sources/receivers cover only a limited angle of view. In this case, the reconstruction of the GPTs becomes more ill-posed than in the full-view case.

It is the aim of this paper to provide a fast algorithm for tracking both the location and the orientation of a mobile target, and precisely analyze the stability of the inverse problem in the limited-view setting.

The paper is organized as follows. In section 2 we recall the conductivity problem and the linear system relating the CGPTs with the MSR data, and provide a stability result in the full angle of view setting. In section 3 we present a GPT-based location and orientation tracking algorithm using an extended Kalman filter and show the numerical results in the

full-view setting. In section 4 we analyze the stability of the CGPT-reconstruction in the limited-view setting and also test the performance of the tracking algorithm. The paper ends with a few concluding remarks. An appendix is for a brief review of the extended Kalman filter.

2 Conductivity problem and reconstruction of CGPTs

We consider the two-dimensional conductivity problem. Let B be a bounded \mathcal{C}^2 -domain of characteristic size of order 1 and centered at the origin. Then $D = z + \delta B$ is an inclusion of characteristic size of order δ and centered at z . We denote by $0 < \kappa \neq 1 < +\infty$ its conductivity, and $\lambda := (\kappa + 1)/(2\kappa - 2)$ its contrast. In the circular setting, N coincident sources/receivers are evenly spaced on the circle of radius R and centered at the origin O between the angular range $(0, \gamma]$. In the full-view case, $\gamma = 2\pi$ while $\gamma < 2\pi$ in the limited-view configuration. The position of s -th source (and r -th receiver) is denoted by x_s (and x_r , respectively) for $s, r = 1 \dots N$, with $\theta_s = \gamma s/N$ the angular position. We require that the circle is large enough to include the inclusion ($R > \delta$). In the following, we set $\rho := R/\delta > 1$.

2.1 CGPTs and the linear system

In the presence of D , the electrical potential u_s resulting from a source at x_s is given as the solution to the following conductivity problem [2]:

$$\begin{cases} \nabla \cdot ((1 + (\kappa - 1)\chi_D)\nabla u_s)(x) = 0, & x \in \mathbb{R}^2, \\ u_s(x) - \Gamma(x - x_s) = O(|x|^{-1}), & |x| \rightarrow +\infty, \end{cases} \quad (1)$$

where $\Gamma(x) = (1/2\pi) \log|x|$ is the fundamental solution of the Laplacian in \mathbb{R}^2 : $\Delta\Gamma(x) = \delta_0(x)$, with δ_0 being the Dirac mass at 0.

Using asymptotic expansion of the fundamental solution, the MSR data $\mathbf{V} = (V_{sr})_{s,r}$ being defined as $V_{sr} = u_s(x_r) - \Gamma(x_r - x_s)$, is linearly related to the GPTs of B as [4, 6]:

$$V_{sr} = \sum_{|\alpha|, |\beta|=1}^K \frac{\delta^{|\alpha|+|\beta|}}{\alpha! \beta!} \partial^\alpha \Gamma(z - x_s) M_{\alpha\beta}(\lambda, B) \partial^\beta \Gamma(z - x_r) + E_{sr} + W_{sr}, \quad (2)$$

where K denotes the highest order of GPTs in the expansion, $\mathbf{E} = (E_{sr})_{s,r}$ the truncation error (non-zero if $K < \infty$), and $\mathbf{W} = (W_{sr})_{s,r}$ the measurement noise following independently the same normal distribution: $W_{sr} \stackrel{\text{iid}}{\sim} \mathcal{N}(0, \sigma_{\text{noise}}^2)$, of mean zero and variance σ_{noise}^2 .

The contracted GPTs, being defined as a harmonic combination of the GPTs [8], allow us to put (2) into an equivalent form [2]:

$$V_{sr} = \sum_{m,n=1}^K \underbrace{\frac{1}{2\pi m \rho^m} (\cos m\theta_s, \sin m\theta_s)}_{\mathbf{A}_{sm}} \underbrace{\begin{pmatrix} \mathbf{M}_{mn}^{cc} & \mathbf{M}_{mn}^{cs} \\ \mathbf{M}_{mn}^{sc} & \mathbf{M}_{mn}^{ss} \end{pmatrix}}_{\mathbf{M}_{mn}} \underbrace{\begin{pmatrix} \cos n\theta_r \\ \sin n\theta_r \end{pmatrix} \frac{1}{2\pi n \rho^n}}_{(\mathbf{A}_{rn})^\top} + E_{sr} + W_{sr}, \quad (3)$$

where \top denotes the transpose and the CGPT matrix $\mathbf{M} = (\mathbf{M}_{mn})_{m,n}$ ¹ has dimension $2K \times 2K$.

Recall that $\mathbf{A} = \mathbf{C}\mathbf{D}$, with \mathbf{C} being a $N \times 2K$ matrix constructed from the block $\mathbf{C}_{rm} = (\cos m\theta_r, \sin m\theta_r)$ and \mathbf{D} a $2K \times 2K$ diagonal matrix:

$$\mathbf{C} = \begin{pmatrix} \mathbf{C}_{11} & \mathbf{C}_{12} & \cdots & \mathbf{C}_{1K} \\ \mathbf{C}_{21} & \mathbf{C}_{22} & \cdots & \mathbf{C}_{2K} \\ \cdots & \cdots & \ddots & \cdots \\ \mathbf{C}_{N1} & \mathbf{C}_{N2} & \cdots & \mathbf{C}_{NK} \end{pmatrix}; \mathbf{D} = \frac{1}{2\pi} \begin{pmatrix} \mathbf{I}_2/\rho & & & \\ & \mathbf{I}_2/(2\rho^2) & & \\ & & \ddots & \\ & & & \mathbf{I}_2/(K\rho^K) \end{pmatrix}. \quad (4)$$

Here, \mathbf{I}_2 is the 2×2 identity matrix. With these notations in hand, we introduce the linear operator

$$\mathbf{L}(\mathbf{M}) = \mathbf{C}\mathbf{D}\mathbf{M}\mathbf{D}\mathbf{C}^\top, \quad (5)$$

and rewrite (3) as:

$$\mathbf{V} = \mathbf{L}(\mathbf{M}) + \mathbf{E} + \mathbf{W}. \quad (6)$$

In order to reconstruct \mathbf{M} , we solve the least-squares problem:

$$\min_{\mathbf{M}} \|\mathbf{L}(\mathbf{M}) - \mathbf{V}\|_F^2, \quad (7)$$

where $\|\cdot\|_F$ denotes the Frobenius norm. It is well known that (7) admits a unique minimal norm solution $\mathbf{M}^{\text{est}} = \mathbf{L}^\dagger(\mathbf{V})$, with \mathbf{L}^\dagger being the pseudo-inverse of \mathbf{L} provided by the following lemma:

Lemma 2.1. *Let \mathbf{A}, \mathbf{B} be two real matrices of arbitrary dimension, and define the linear operator $\mathbf{L}(\mathbf{X}) = \mathbf{A}\mathbf{X}\mathbf{B}^\top$. If $\mathbf{A}^\dagger, \mathbf{B}^\dagger$ are the pseudo-inverse of \mathbf{A}, \mathbf{B} respectively, then the pseudo-inverse of \mathbf{L} is given by*

$$\mathbf{L}^\dagger(\mathbf{Y}) = \mathbf{A}^\dagger\mathbf{Y}(\mathbf{B}^\dagger)^\top. \quad (8)$$

Proof. This is a straightforward verification of the definition of pseudo-inverse, namely: 1) $\mathbf{L}^\dagger\mathbf{L}$ and $\mathbf{L}\mathbf{L}^\dagger$ are self-adjoint; 2) $\mathbf{L}\mathbf{L}^\dagger\mathbf{L} = \mathbf{L}$ and $\mathbf{L}^\dagger\mathbf{L}\mathbf{L}^\dagger = \mathbf{L}^\dagger$. For the first point:

$$\mathbf{L}^\dagger(\mathbf{L}(\mathbf{X})) = \mathbf{A}^\dagger\mathbf{A}\mathbf{X}(\mathbf{B}^\dagger\mathbf{B})^\top,$$

which is self-adjoint since the matrices $\mathbf{A}^\dagger\mathbf{A}$ and $\mathbf{B}^\dagger\mathbf{B}$ are symmetric by definition of pseudo-inverse; while for the second point, it follows from the definition again that

$$\mathbf{L}(\mathbf{L}^\dagger(\mathbf{L}(\mathbf{X}))) = \mathbf{A}\mathbf{A}^\dagger\mathbf{A}\mathbf{X}(\mathbf{B}\mathbf{B}^\dagger\mathbf{B})^\top = \mathbf{A}\mathbf{X}\mathbf{B}^\top = \mathbf{L}(\mathbf{X}).$$

Similarly, one can verify the self-adjointness of $\mathbf{L}\mathbf{L}^\dagger$ and $\mathbf{L}^\dagger\mathbf{L}\mathbf{L}^\dagger = \mathbf{L}^\dagger$. \square

¹Throughout the paper, we will write \mathbf{M}_{mn} for the m, n -th 2×2 building block, and $(\mathbf{M})_{ab}$ for the a, b -th entry in \mathbf{M} .

2.2 Full-view setting

In [2], we have investigated the resolving order of CGPT reconstruction in the full angle of view setting: $\gamma = 2\pi$. Given $N \geq 2K$, it has been shown that the matrix \mathbf{C} is orthogonal (up to the factor $N/2$):

$$\mathbf{C}^\top \mathbf{C} = \frac{N}{2} \mathbf{I},$$

and the pseudo-inverse solution takes the form:

$$\mathbf{L}^\dagger(\mathbf{V}) = \frac{4}{N^2} \mathbf{D}^{-1} \mathbf{C}^\top \mathbf{V} \mathbf{C} \mathbf{D}^{-1}. \quad (9)$$

Furthermore, the reconstruction problem is exponentially ill-posed. More precisely, the following result holds.

Proposition 2.2. *Let \mathbf{e}_{ab} be the $2K \times 2K$ matrix whose elements are all zero but the (a, b) th element is equal to 1. In the circular and full-view setting with $N \geq 2K$, the (a, b) -th singular value of the operator \mathbf{L} , for $a, b = 1, \dots, 2K$, is*

$$\lambda_{ab} = N / (8\pi^2 \lceil a/2 \rceil \lceil b/2 \rceil \rho^{\lceil a/2 \rceil + \lceil b/2 \rceil}), \quad (10)$$

with the matrix \mathbf{e}_{ab} as the right singular vector, and $\mathbf{f}_{ab} = \lambda_{ab}^{-1} \mathbf{L}(\mathbf{e}_{ab})$ as the left singular vector. In particular, the condition number of the operator \mathbf{L} is $K^2 \rho^{2(K-1)}$.

Proof. Using the fact that $\mathbf{C}^\top \mathbf{C} = \frac{N}{2} \mathbf{I}$, we have, for any square matrices \mathbf{U} and \mathbf{V} ,

$$\langle \mathbf{L}(\mathbf{U}), \mathbf{L}(\mathbf{V}) \rangle = \frac{N^2}{4} \langle \mathbf{D} \mathbf{U} \mathbf{D}, \mathbf{D} \mathbf{V} \mathbf{D} \rangle, \quad (11)$$

where $\langle \cdot, \cdot \rangle$ is the termwise inner product. Since \mathbf{D} is diagonal and invertible, we conclude that the canonical basis $\{\mathbf{e}_{ab}\}_{a,b}$ is the singular vector of \mathbf{L} , and the associated singular value is $\|\mathbf{L}(\mathbf{e}_{ab})\|_F = \|\mathbf{D} \mathbf{e}_{ab} \mathbf{D}\|_F N/2 = N / (8\pi^2 \lceil a/2 \rceil \lceil b/2 \rceil \rho^{\lceil a/2 \rceil + \lceil b/2 \rceil})$. \square

As a simple consequence, we have $\mathbf{L}^\dagger(\mathbf{W})_{ab} = \lambda_{ab}^{-1} \langle \mathbf{W}, \mathbf{f}_{ab} \rangle$. When K is sufficiently large, the truncation error \mathbf{E} is $O(\rho^{-K-2})$ and can be neglected if compared to \mathbf{W} [2], and then by the property of white noise

$$\sqrt{\mathbb{E}(((\mathbf{M}^{\text{est}})_{ab} - (\mathbf{M})_{ab})^2)} \lesssim \sqrt{\mathbb{E}((\mathbf{L}^\dagger(\mathbf{W})_{ab})^2)} = \lambda_{ab}^{-1} \sigma_{\text{noise}},$$

which is the result already established in [2]. Hence, it follows from (10) that the reconstruction of high order CGPTs is an ill-posed problem. Nonetheless the system has the remarkable property that low order CGPTs are not affected by the error caused by the instability of higher orders as the following proposition shows.

Proposition 2.3. *Let \mathbf{M}_K denote the CGPTs of order up to K , and let \mathbf{L}_K be the corresponding linear operator in (3). Then, for any order $K_1 \leq K_2 < N/2$, the submatrix of $\mathbf{L}_{K_2}^\dagger(\mathbf{V})$ formed by the first $2K_1$ columns and rows is identical to the minimal norm solution $\mathbf{L}_{K_1}^\dagger(\mathbf{V})$.*

Proof. Let the $N \times 2K$ matrix J_K be the row concatenation of the $2K \times 2K$ identity matrix \mathbf{I}_{2K} and a zero matrix. We have $\mathbf{J}_K^\top \mathbf{J}_K = \mathbf{I}_{2K}$ and $\mathbf{J}_{K_1}^\top \mathbf{L}_{K_2}^\dagger(\mathbf{V}) \mathbf{J}_{K_1}$ is the submatrix of $\mathbf{L}_{K_2}^\dagger(\mathbf{V})$ formed by the first $2K_1$ columns and rows. Let \mathbf{D}_K and \mathbf{C}_K be the matrices defined in (4). Because of (9), we have

$$\mathbf{J}_{K_1}^\top \mathbf{L}_{K_2}^\dagger(\mathbf{V}) \mathbf{J}_{K_1} = \frac{4}{N^2} \mathbf{J}_{K_1}^\top \mathbf{D}_{K_2}^{-1} \mathbf{C}_{K_2}^\top \mathbf{V} \mathbf{C}_{K_2} \mathbf{D}_{K_2}^{-1} \mathbf{J}_{K_1}.$$

One can easily see that

$$\mathbf{C}_{K_2} \mathbf{D}_{K_2}^{-1} \mathbf{J}_{K_1} = \mathbf{C}_{K_1} \mathbf{D}_{K_1}^{-1}.$$

Thus, we have

$$\mathbf{J}_{K_1}^\top \mathbf{L}_{K_2}^\dagger(\mathbf{V}) \mathbf{J}_{K_1} = \mathbf{L}_{K_1}^\dagger(\mathbf{V}).$$

□

Numerically, \mathbf{L}^\dagger can be implemented through either the formula (9) or the Conjugated Gradient (CG) method using (7). Simulations in [2] confirm that in typical situations, say, with $K = 5$ and 10% noise, the reconstructed CGPT is sufficiently accurate for the task such as the target identification in a dictionary. In the next section we present a location and orientation tracking algorithm for a mobile target based on the concept of CGPTs.

3 Tracking of a mobile target

At the instant $t \geq 0$, we denote by $z_t = [x_t, y_t]^\top \in \mathbb{R}^2$ the location and $\theta_t \in [0, 2\pi)$ the orientation of a target D_t .

$$D_t = z_t + R_{\theta_t} D, \quad (12)$$

where R_{θ_t} is the rotation by θ_t . Let \mathbf{M}_t be the CGPT of D_t , and \mathbf{M}_D be the CGPT of D . Then the equation (6) becomes:

$$\mathbf{V}_t = \mathbf{L}(\mathbf{M}_t) + \mathbf{E}_t + \mathbf{W}_t, \quad (13)$$

where \mathbf{E}_t is the truncation error, and \mathbf{W}_t the measurement noise at time t .

The objective of *tracking* is to estimate the target's location z_t and orientation θ_t from the MSR data stream \mathbf{V}_t . We emphasize that these informations are contained in the first two orders CGPTs as shown in the previous paper [2]. Precisely, let $\Delta x_t = x_t - x_{t-1}$, $\Delta y_t = y_t - y_{t-1}$ and $\Delta \theta_t = \theta_t - \theta_{t-1}$, then the following relations (when it is well defined) exist between the CGPT of D_t and D_{t-1} [2]:

$$\begin{aligned} \mathbf{N}_{12}^{(1)}(D_t)/\mathbf{N}_{11}^{(1)}(D_t) &= 2(\Delta x_t + i\Delta y_t) + e^{i\Delta \theta_t} \mathbf{N}_{12}^{(1)}(D_{t-1})/\mathbf{N}_{11}^{(1)}(D_{t-1}), \\ \mathbf{N}_{12}^{(2)}(D_t)/\mathbf{N}_{11}^{(2)}(D_t) &= 2(\Delta x_t + i\Delta y_t) + e^{i\Delta \theta_t} \mathbf{N}_{12}^{(2)}(D_{t-1})/\mathbf{N}_{11}^{(2)}(D_{t-1}). \end{aligned} \quad (14)$$

Hence when the linear system (14) is solvable, one can estimate z_t, θ_t by solving and accumulating $\Delta x_t, \Delta y_t$ and $\Delta \theta_t$. However, such an algorithm will propagate the error over time, since the noise presented in data is not properly taken into account here.

In the following we develop a CGPT-based tracking algorithm using the Extended Kalman Filter, which handles correctly the noise. We recall first the definition of complex CGPT, with which a simple relation between \mathbf{M}_t and \mathbf{M}_D can be established.

3.1 Time relationship between CGPTs

Let $u = (1, i)^\top$. The complex CGPTs $\mathbf{N}^{(1)}, \mathbf{N}^{(2)}$ are defined by

$$\begin{aligned}\mathbf{N}_{mn}^{(1)} &= (M_{mn}^{cc} - M_{mn}^{ss}) + i(M_{mn}^{cs} + M_{mn}^{sc}) = u^\top \mathbf{M}_{mn} u, \\ \mathbf{N}_{mn}^{(2)} &= (M_{mn}^{cc} + M_{mn}^{ss}) + i(M_{mn}^{cs} - M_{mn}^{sc}) = u^H \mathbf{M}_{mn} u,\end{aligned}$$

where H denotes the Hermitian transpose. Therefore, we have

$$\mathbf{N}^{(1)} = \mathbf{U}^\top \mathbf{M} \mathbf{U} \quad \text{and} \quad \mathbf{N}^{(2)} = \mathbf{U}^H \mathbf{M} \mathbf{U}, \quad (15)$$

where the matrix \mathbf{U} of dimension $2K \times K$ over the complex fields is defined by

$$\mathbf{U} = \begin{pmatrix} u & 0 & \dots & 0 \\ 0 & u & \dots & 0 \\ \vdots & & \ddots & \vdots \\ 0 & \dots & 0 & u \end{pmatrix}. \quad (16)$$

It is worth mentioning that $\mathbf{N}^{(1)}$ and $\mathbf{N}^{(2)}$ are complex matrices of dimension $K \times K$.

To recover the CGPT \mathbf{M}_{mn} from the complex CGPTs $\mathbf{N}^{(1)}, \mathbf{N}^{(2)}$, we simply use the relations

$$\begin{aligned}M_{mn}^{cc} &= \frac{1}{2} \Re(\mathbf{N}_{mn}^{(1)} + \mathbf{N}_{mn}^{(2)}), \quad M_{mn}^{cs} = \frac{1}{2} \Im(\mathbf{N}_{mn}^{(1)} + \mathbf{N}_{mn}^{(2)}), \\ M_{mn}^{sc} &= \frac{1}{2} \Im(\mathbf{N}_{mn}^{(1)} - \mathbf{N}_{mn}^{(2)}), \quad M_{mn}^{ss} = \frac{1}{2} \Re(\mathbf{N}_{mn}^{(2)} - \mathbf{N}_{mn}^{(1)}),\end{aligned} \quad (17)$$

where \Re, \Im are the real and imaginary part of a complex number, respectively. For two targets D_t, D satisfying (12), the following relationships between their complex CGPT hold [2]:

$$\mathbf{N}^{(1)}(D_t) = F_t^\top \mathbf{N}^{(1)}(D) F_t, \quad (18a)$$

$$\mathbf{N}^{(2)}(D_t) = F_t^H \mathbf{N}^{(2)}(D) F_t, \quad (18b)$$

where F_t is a upper triangle matrix with the (m, n) -th entry given by

$$(F_t)_{mn} = \binom{n}{m} (x_t + iy_t)^{n-m} e^{im\theta_t}. \quad (19)$$

Linear operator \mathbf{T}_t : Now one can find explicitly a linear operator \mathbf{T}_t (the underlying scalar field is \mathbb{R}) which depends only on z_t, θ_t , such that $\mathbf{M}_t = \mathbf{T}_t(\mathbf{M}_D)$, and the equation (13) becomes

$$\mathbf{V}_t = \mathbf{L}(\mathbf{T}_t(\mathbf{M}_D)) + \mathbf{E}_t + \mathbf{W}_t. \quad (20)$$

For doing so, we set $J_t := \mathbf{U} F_t$, where \mathbf{U} is given by (16). Then, a straightforward computation using (15), (17), and (18) shows that

$$\begin{aligned}M^{cc}(D_t) &= \Re J_t^\top \mathbf{M}_D \Re J_t, \quad M^{cs}(D_t) = \Re J_t^\top \mathbf{M}_D \Im J_t, \\ M^{sc}(D_t) &= \Im J_t^\top \mathbf{M}_D \Re J_t, \quad M^{ss}(D_t) = \Im J_t^\top \mathbf{M}_D \Im J_t,\end{aligned} \quad (21)$$

where $M^{cc}(D_t), M^{cs}(D_t), M^{sc}(D_t), M^{ss}(D_t)$ are defined in (3). Therefore, we get the operator \mathbf{T}_t :

$$\begin{aligned} \mathbf{T}_t(\mathbf{M}_D) &= \Re\mathbf{U}(\Re J_t^\top \mathbf{M}_D \Re J_t) \Re\mathbf{U}^\top + \Re\mathbf{U}(\Re J_t^\top \mathbf{M}_D \Im J_t) \Im\mathbf{U}^\top + \\ &\quad \Im\mathbf{U}(\Im J_t^\top \mathbf{M}_D \Re J_t) \Re\mathbf{U}^\top + \Im\mathbf{U}(\Im J_t^\top \mathbf{M}_D \Im J_t) \Im\mathbf{U}^\top = \mathbf{M}_t. \end{aligned} \quad (22)$$

3.2 Tracking by the Extended Kalman Filter

The EKF is a generalization of the KF to nonlinear dynamical systems. Unlike KF which is an optimal estimator for linear systems with Gaussian noise, EKF is no longer optimal, but it remains robust with respect to noise and computationally inexpensive, therefore is well suited for real-time applications such as tracking. We establish here the *system state* and the *observation* equations which are fundamental to EKF, and refer readers to Appendix B for its algorithmic details.

3.2.1 System state observation equations

We assume that the position of the target is subjected to an external driving force that has the form of a white noise. In other words the velocity $(V(\tau))_{\tau \in \mathbb{R}^+}$ of the target is given in terms of a two-dimensional Brownian motion $(W_a(\tau))_{\tau \in \mathbb{R}^+}$ and its position $(Z(\tau))_{\tau \in \mathbb{R}^+}$ is given in terms of the integral of this Brownian motion:

$$V(\tau) = V_0 + \sigma_a W_a(\tau), \quad Z(\tau) = Z_0 + \int_0^\tau V(s) ds.$$

The orientation $(\Theta(\tau))_{\tau \in \mathbb{R}^+}$ of the target is subjected to random fluctuations and its angular velocity is given in terms of an independent white noise, so that the orientation is given in terms of a one-dimensional Brownian motion $(W_\theta(\tau))_{\tau \in \mathbb{R}^+}$:

$$\Theta(\tau) = \Theta_0 + \sigma_\theta W_\theta(\tau).$$

We observe the target at discrete times $t\Delta\tau$, $t \in \mathbb{N}$, with time step $\Delta\tau$. We denote $z_t = Z(t\Delta\tau)$, $v_t = V(t\Delta\tau)$, and $\theta_t = \Theta(t\Delta\tau)$. They obey the recursive relations

$$\begin{aligned} v_t &= v_{t-1} + a_t, & a_t &= \sigma_a (W_a(t\Delta\tau) - W_a((t-1)\Delta\tau)), \\ z_t &= z_{t-1} + v_{t-1}\Delta\tau + b_t, & b_t &= \sigma_a \int_{(t-1)\Delta\tau}^{t\Delta\tau} W_a(s) - W_a((t-1)\Delta\tau) ds, \\ \theta_t &= \theta_{t-1} + c_t, & c_t &= \sigma_\theta (W_\theta(t\Delta\tau) - W_\theta((t-1)\Delta\tau)). \end{aligned} \quad (23)$$

Since the increments of the Brownian motions are independent from each other, the vectors $(U_t)_{t \geq 1}$ given by

$$U_t = \begin{pmatrix} a_t \\ b_t \\ c_t \end{pmatrix}$$

are independent and identically distributed with the multivariate normal distribution with mean zero and covariance matrix Σ given by

$$\Sigma = \Delta\tau \begin{pmatrix} \sigma_a^2 \mathbf{I}_2 & \frac{\sigma_a^2}{2} \Delta\tau \mathbf{I}_2 & 0 \\ \frac{\sigma_a^2}{2} \Delta\tau \mathbf{I}_2 & \frac{\sigma_a^2}{3} \Delta\tau^2 \mathbf{I}_2 & 0 \\ 0 & 0 & \sigma_\theta^2 \end{pmatrix} \quad (24)$$

The evolution of the state vector

$$X_t = \begin{pmatrix} v_t \\ z_t \\ \theta_t \end{pmatrix}$$

takes the form

$$X_t = \mathbf{F}X_{t-1} + U_t, \quad \mathbf{F} = \begin{pmatrix} \mathbf{I}_2 & 0 & 0 \\ \Delta\tau\mathbf{I}_2 & \mathbf{I}_2 & 0 \\ 0 & 0 & 1 \end{pmatrix} \quad (25)$$

The observation made at time t is the MSR matrix given by (20), where the system state X_t is implicitly included in the operator \mathbf{T}_t . We suppose that the truncation error \mathbf{E}_t is small compared to the measurement noise so that it can be dropped in (20), and that the Gaussian white noise \mathbf{W}_t of different time are mutually independent. We emphasize that the velocity vector v_t of the target does not contribute to (20), which can be seen from (12). To highlight the dependence upon z_t, θ_t , we introduce a function h which is nonlinear in z_t, θ_t , and takes \mathbf{M}_D as a parameter, such that

$$h(X_t; \mathbf{M}_D) = h(z_t, \theta_t; \mathbf{M}_D) = \mathbf{L}(\mathbf{T}_t(\mathbf{M}_D)). \quad (26)$$

Then together with (25) we get the following *system state* and *observation* equations:

$$X_t = \mathbf{F}X_{t-1} + U_t, \quad (27a)$$

$$\mathbf{V}_t = h(X_t; \mathbf{M}_D) + \mathbf{W}_t. \quad (27b)$$

Note that (27a) is linear, so in order to apply EKF on (27), we only need to linearize (27b), or in other words, to calculate the partial derivatives of h with respect to x_t, y_t, θ_t .

3.2.2 Linearization of the observation equation

Clearly, the operator \mathbf{L} contains only the information concerning the acquisition system and does not depend on x_t, y_t, θ_t . So by (26), we have

$$\partial_{x_t} h = \mathbf{L}(\partial_{x_t} \mathbf{T}_t(\mathbf{M}_D)), \quad (28)$$

while the calculation for $\partial_{x_t} \mathbf{T}_t$ is straightforward using (22). We have

$$\begin{aligned} \partial_{x_t} \mathbf{T}_t(\mathbf{M}_D) = & \Re\mathbf{U}\partial_{x_t}(\Re J_t^\top \mathbf{M}_D \Re J_t) \Re\mathbf{U}^\top + \Re\mathbf{U}\partial_{x_t}(\Re J_t^\top \mathbf{M}_D \Im J_t) \Im\mathbf{U}^\top + \\ & \Im\mathbf{U}\partial_{x_t}(\Im J_t^\top \mathbf{M}_D \Re J_t) \Re\mathbf{U}^\top + \Im\mathbf{U}\partial_{x_t}(\Im J_t^\top \mathbf{M}_D \Im J_t) \Im\mathbf{U}^\top, \end{aligned} \quad (29)$$

where the derivatives are found by the chain rule:

$$\begin{aligned} \partial_{x_t}(\Re J_t^\top \mathbf{M}_D \Re J_t) &= \Re(\partial_{x_t} J_t^\top) \mathbf{M}_D \Re J_t + \Re J_t^\top \mathbf{M}_D \Re(\partial_{x_t} J_t), \\ \partial_{x_t}(\Re J_t^\top \mathbf{M}_D \Im J_t) &= \Re(\partial_{x_t} J_t^\top) \mathbf{M}_D \Im J_t + \Re J_t^\top \mathbf{M}_D \Im(\partial_{x_t} J_t), \\ \partial_{x_t}(\Im J_t^\top \mathbf{M}_D \Re J_t) &= \Im(\partial_{x_t} J_t^\top) \mathbf{M}_D \Re J_t + \Im J_t^\top \mathbf{M}_D \Re(\partial_{x_t} J_t), \\ \partial_{x_t}(\Im J_t^\top \mathbf{M}_D \Im J_t) &= \Im(\partial_{x_t} J_t^\top) \mathbf{M}_D \Im J_t + \Im J_t^\top \mathbf{M}_D \Im(\partial_{x_t} J_t), \end{aligned}$$

and $\partial_{x_t} J_t = \mathbf{U}\partial_{x_t} \mathbf{F}_t$. The (m, n) -th entry of the matrix $\partial_{x_t} \mathbf{F}_t$ is given by

$$(\partial_{x_t} \mathbf{F}_t)_{m,n} = \binom{n}{m} (n-m) z_t^{n-m-1} e^{im\theta_t}. \quad (30)$$

The derivatives $\partial_{y_t} \mathbf{T}_t(\mathbf{M}_D)$ and $\partial_{\theta_t} \mathbf{T}_t(\mathbf{M}_D)$ are calculated in the same way.

3.3 Numerical experiments of tracking in the full-view setting

Here we show the performance of EKF in a full angle of view setting with the shape 'A' as target D , which has diameter 10 and is centered at the origin. The path (z_t, θ_t) is simulated according to the model (23) during a period of 10 seconds ($\Delta\tau = 0.01$), with parameters $\sigma_a = 2, \sigma_\theta = 0.5$, and the initial state $X_0 = (v_0, z_0, \theta_0)^\top = (-1, 1, 5, -5, 3\pi/2)^\top$. We make sure that the target is always included inside the measurement circle on which $N = 20$ sources/receivers are fixed, see Fig. 1. The data stream \mathbf{V}_t is generated by first calculating the MSR matrix corresponding to each $D_t, t \geq 0$ then adding a white noise.

Suppose that the CGPT of D is correctly determined (for instance, by identifying the target in a dictionary [2]). Then we use the first two orders CGPT \mathbf{M}_D of D in (27b), and take $(0, 0, 10, -0.5, 0)^\top$ as initial guess of X_0 for EKF.

We add 10% and 20% of noise to data, and show the results of tracking in Fig. 2 (a) (c) and (e). We see that EKF can find the true system state, despite of the poor initial guess, and the tracking precision decays as the measurement noise level gets higher. The same experiment with small target (of same shape) of diameter 1 is repeated in Fig. 2 (b) (d) and (f), where the tracking of position remains correct, on the contrary, that of orientation fails when the noise level is high. Such a result is in accordance with physical intuitions. In fact, the position of a small target can be easily localized in the far field, while its orientation can be correctly determined only in the near field.

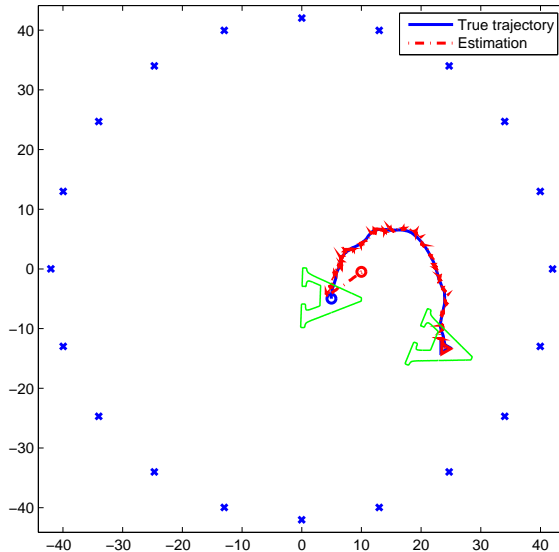


Figure 1: Trajectory of the letter 'A' and the estimation by EKF. The initial position is $(5, -5)$ while the initial guess given to EKF is $(10, -0.5)$. The crosses indicate the position of sources/receivers, while the circle and the triangle indicate the starting and the final position of the target, respectively. In blue is the true trajectory and in red the estimated one.

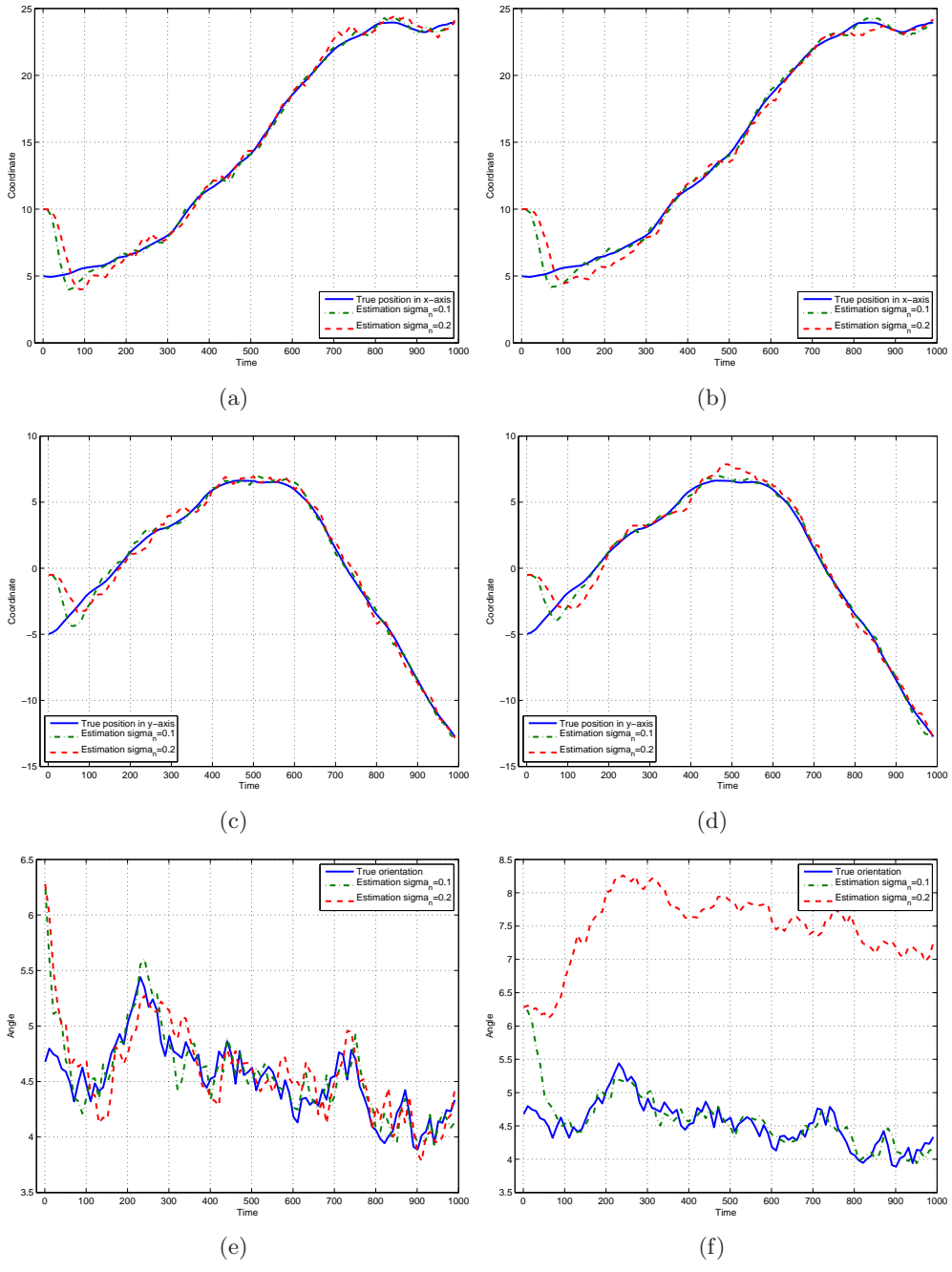


Figure 2: Results of tracking using the configuration of Fig. 1 at different noise levels. First row: coordinate in x -axis. Second row: coordinate in y -axis. Last row: orientation. In the first column the target has size 10, while in the second column the target has size 1. The solid line always indicates the true system state.

4 CGPT reconstruction and tracking problem in the limited-view setting

In this section we study the stability of CGPTs reconstruction and tracking problem in the case $0 < \gamma < 2\pi$, always under the condition that $N > 2K$, *i.e.*, the number of sources/receivers is two times larger than the highest order of CGPTs to be reconstructed. Unlike in the full-view case, here \mathbf{C} is no longer orthogonal in general, nonetheless one can still establish the SVD of \mathbf{L} similarly as in Proposition 2.2.

Proposition 4.1. *Consider the concentric and limited-view setting with $N \geq 2K$, and suppose that \mathbf{C} is of maximal rank. Let $\{\mu_n\}$ be the n -th largest eigenvalue of the matrix $\mathbf{DC}^\top \mathbf{CD}$ and let $\{v_n\}$ be the associated orthonormal eigenvector. Then the (a, b) -th singular value of the operator \mathbf{L} is $\lambda_{ab} = \sqrt{\mu_a \mu_b}$, with the associated left singular vector the matrix $\mathbf{g}_{ab} = v_a v_b^\top$. In particular, the condition number of the operator \mathbf{L} is*

$$\text{cond}(\mathbf{L}) = \text{cond}(\mathbf{DC}^\top \mathbf{CD}) \leq \text{cond}(\mathbf{C})^2 K^2 \rho^{2(K-1)}, \quad (31)$$

with $\text{cond}(\mathbf{C})$ being the condition number of the matrix \mathbf{C} .

Proof. We first note that for any matrices \mathbf{U}, \mathbf{V} we have:

$$\langle \mathbf{L}(\mathbf{U}), \mathbf{L}(\mathbf{V}) \rangle = \langle \mathbf{U}, (\mathbf{DC}^\top \mathbf{CD})\mathbf{V}(\mathbf{DC}^\top \mathbf{CD}) \rangle.$$

Taking $\mathbf{g}_{ab} = v_a v_b^\top$, and $\mathbf{g}_{a'b'} = v_{a'} v_{b'}^\top$, we get

$$\begin{aligned} \langle \mathbf{L}(\mathbf{g}_{ab}), \mathbf{L}(\mathbf{g}_{a'b'}) \rangle &= \mu_{a'} \langle v_a v_b^\top, v_{a'} v_{b'}^\top (\mathbf{DC}^\top \mathbf{CD}) \rangle = \mu_{a'} \mu_{b'} \langle v_a v_b^\top, v_{a'} v_{b'}^\top \rangle \\ &= \delta_{aa'} \delta_{bb'} \mu_a \mu_b, \end{aligned}$$

where $\delta_{aa'}$ is the Kronecker's symbol, which implies that $\|\mathbf{L}(\mathbf{g}_{ab})\|_F = \sqrt{\mu_a \mu_b}$ is the (a, b) -th singular value of \mathbf{L} . We denote by $\rho_{\max}(\cdot), \rho_{\min}(\cdot)$ the maximal and the minimal singular values of a matrix, then

$$\begin{aligned} \rho_{\max}(\mathbf{DC}^\top \mathbf{CD}) &= \rho_{\max}(\mathbf{CD})^2 \leq \rho_{\max}(\mathbf{C})^2 \rho_{\max}(\mathbf{D})^2, \\ \rho_{\min}(\mathbf{DC}^\top \mathbf{CD}) &= \rho_{\min}(\mathbf{CD})^2 \geq \rho_{\min}(\mathbf{C})^2 \rho_{\min}(\mathbf{D})^2, \end{aligned}$$

and the condition number of \mathbf{L} is therefore bounded by $\text{cond}(\mathbf{C})^2 K^2 \rho^{2(K-1)}$. \square

4.1 Injectivity of \mathbf{C}

We denote by V_K the vector space of functions of the form

$$f(\theta) = \sum_{k=-K}^K c_k e^{ik\theta}, \quad (32)$$

with $c_k \in \mathbb{C}$, and V_K^0 the subspace of V_K such that $c_0 = 0$. Functions of V_K^0 can be written as

$$f(\theta) = \sum_{k=1}^K \alpha_k \cos(k\theta) + \beta_k \sin(k\theta), \quad (33)$$

with $\alpha_k, \beta_k \in \mathbb{C}$. Observe that taking discrete samples of (33) at $\theta_s = \gamma s/N$ is nothing but applying the matrix \mathbf{C} on a coefficient vector $(\alpha_1, \beta_1 \dots \alpha_K, \beta_K)$. We have the following result.

Proposition 4.2. *For any $N \geq 2K$, the matrix \mathbf{C} is of maximal rank.*

Proof. Multiplying $f \in V_K^0$ in (32) by $e^{iK\theta}$, and using the fact that $c_0 = 0$, we have

$$\begin{aligned} e^{iK\theta} f(\theta) &= \sum_{k=0}^{K-1} c_{k-K} e^{ik\theta} + \sum_{k=K+1}^{2K} c_{k-K} e^{ik\theta} \\ &= \sum_{k=0}^{K-1} c_{k-K} e^{ik\theta} + \sum_{k=K}^{2K-1} e^{i\theta} c_{k+1-K} e^{ik\theta} = \sum_{k=0}^{2K-1} \tilde{c}_k e^{ik\theta}, \end{aligned} \quad (34)$$

where $\tilde{c}_k = c_{k-K}$ for $k = 0, \dots, K-1$, and $\tilde{c}_k = e^{i\theta} c_{k+1-K}$ for $k = K, \dots, 2K-1$. The N vectors $v_s := (e^{ik\theta_s})_{k=0 \dots 2K-1}$ are linearly independent since they are the first $2K \leq N$ rows of a $N \times N$ Vandermonde matrix. Therefore, $f(\theta_s) = 0$ for $s = 1 \dots N$ implies that $\tilde{c}_k = 0$ for all $k = 0, \dots, 2K-1$, which means that \mathbf{C} is of maximal rank. \square

Consequently, for arbitrary range $0 < \gamma \leq 2\pi$, a sufficient condition to uniquely determine the CGPTs of order up to K is to have $N \geq 2K$ sources/receivers.

4.2 Explicit left inverse of \mathbf{C}

We denote by $D_K(\theta)$ the Dirichlet kernel of order K :

$$D_K(\theta) = \sum_{k=-K}^K e^{ik\theta} = \frac{\sin((K+1/2)\theta)}{\sin(\theta/2)}. \quad (35)$$

We state without proof the following well known result about V_K .

Lemma 4.3. *The functions $\{D_K(\theta - \frac{2\pi n}{2K+1})\}_{n=0, \dots, 2K}$ is an orthogonal basis of V_K . For any $f, g \in V_K$, the following identity holds:*

$$\frac{1}{2\pi} \int_0^{2\pi} f(\theta) g^*(\theta) d\theta = \frac{1}{2K+1} \sum_{n=1}^{2K+1} f\left(\frac{2\pi n}{2K+1}\right) g\left(\frac{2\pi n}{2K+1}\right), \quad (36)$$

where $*$ denotes the complex conjugate. In particular, we have for $n = 0, \dots, 2K$

$$\frac{1}{2\pi} \int_0^{2\pi} f(\theta) D_K\left(\theta - \frac{2\pi n}{2K+1}\right) d\theta = f\left(\frac{2\pi n}{2K+1}\right). \quad (37)$$

Lemma 4.4. *Given a set of $N > 2K$ different points $0 < \theta_1 < \dots < \theta_N \leq 2\pi$, there exist interpolation kernels $h_s \in V_{\lfloor N/2 \rfloor}$ for $s = 1 \dots N$, such that:*

$$f(\theta) = \sum_{s=1}^N f(\theta_s) h_s(\theta) \quad \text{for any } f \in V_K. \quad (38)$$

Proof. When the number of points N is odd, it is well known [27] that h_s takes the form

$$h_s(\theta) = \prod_{t=1, t \neq s}^N \frac{\sin\left(\frac{\theta - \theta_t}{2}\right)}{\sin\left(\frac{\theta_s - \theta_t}{2}\right)}. \quad (39)$$

When N is even, by a result established in [22]

$$h_s(\theta) = \cos\left(\frac{\theta - \theta_s}{2}\right) \prod_{t=1, t \neq s}^N \frac{\sin\left(\frac{\theta - \theta_t}{2}\right)}{\sin\left(\frac{\theta_s - \theta_t}{2}\right)}. \quad (40)$$

It is easy to see that in both cases h_s belongs to $V_{\lfloor N/2 \rfloor}$. \square

Now we can find explicitly a left inverse for \mathbf{C} .

Proposition 4.5. *Under the same condition as in Lemma 4.4, we denote by h_s the interpolation kernel and define the matrix $\tilde{\mathbf{C}} = (\tilde{\mathbf{C}}_{ks})_{k,s}$ as*

$$\tilde{\mathbf{C}}_{2k-1,s} = \frac{1}{\pi} \int_0^{2\pi} h_s(\theta) \cos(k\theta) d\theta, \quad \tilde{\mathbf{C}}_{2k,s} = \frac{1}{\pi} \int_0^{2\pi} h_s(\theta) \sin(k\theta) d\theta. \quad (41)$$

Then $\tilde{\mathbf{C}}\mathbf{C} = \mathbf{I}$. In particular, if N is odd, the matrix $\tilde{\mathbf{C}}$ can be calculated as

$$\tilde{\mathbf{C}}_{2k-1,s} = \frac{2}{N} \sum_{n=1}^N h_s\left(\frac{2\pi n}{N}\right) \cos\left(\frac{2\pi kn}{N}\right), \quad \tilde{\mathbf{C}}_{2k,s} = \frac{2}{N} \sum_{n=1}^N h_s\left(\frac{2\pi n}{N}\right) \sin\left(\frac{2\pi kn}{N}\right). \quad (42)$$

Proof. Given $v = (\alpha_1, \beta_1, \dots, \alpha_K, \beta_K) \in \mathbb{C}^{2K}$, and f the associated function defined by (33), we have $(\mathbf{C}v)_n = f(\theta_n)$ for $n = 1, \dots, N$. Using (38) and (41), we find that

$$(\tilde{\mathbf{C}}\mathbf{C}v)_{2k-1} = \frac{1}{\pi} \int_0^{2\pi} f(\theta) \cos(k\theta) d\theta = \alpha_k, \quad (43)$$

$$(\tilde{\mathbf{C}}\mathbf{C}v)_{2k} = \frac{1}{\pi} \int_0^{2\pi} f(\theta) \sin(k\theta) d\theta = \beta_k, \quad (44)$$

and therefore, $\tilde{\mathbf{C}}\mathbf{C}v = v$. Observe that $h_s(\theta)$, $\cos(k\theta)$, and $\sin(k\theta)$ all belong to $V_{\lfloor N/2 \rfloor}$, so when N is odd, we easily deduce (42) using (36). \square

Remark 4.1. In general, the left inverse $\tilde{\mathbf{C}}$ in (41) is not the pseudo-inverse of \mathbf{C} , and by definition, we have $\mathbf{C}^\dagger = \tilde{\mathbf{C}}$ if $\mathbf{C}\tilde{\mathbf{C}}$ is symmetric. If $P_{V_K^0}(h_s)$ is the orthogonal projection of h_s onto V_K^0 , i.e.,

$$P_{V_K^0}(h_s)(\theta) = \sum_{k=1}^K \tilde{\mathbf{C}}_{2k-1,s} \cos(k\theta) + \tilde{\mathbf{C}}_{2k,s} \sin(k\theta), \quad (45)$$

then, $P_{V_K^0}(h_s)(\theta_t) = (\mathbf{C}\tilde{\mathbf{C}})_{st}$. Therefore, $\tilde{\mathbf{C}}$ is the pseudo-inverse of \mathbf{C} if and only if the interpolation kernel h_s satisfies:

$$P_{V_K^0}(h_s)(\theta_t) = P_{V_K^0}(h_t)(\theta_s), \quad \text{for } s, t = 1 \dots N. \quad (46)$$

Remark 4.2. Proposition 4.5 can be used in the noiseless limited-view case to reconstruct the CGPT matrix \mathbf{M} from the MSR measurements \mathbf{V} . In fact, from (5) it immediately follows that

$$\mathbf{M} = \mathbf{D}^{-1} \tilde{\mathbf{C}} \mathbf{V} \tilde{\mathbf{C}}^\top \mathbf{D}^{-1}.$$

This shows that in the noiseless case, the limited-view aspect has no effect on the reconstruction of the GPTs, and consequently on the location and orientation tracking. In the presence of noise, the effect, as will be shown in the next subsection, is dramatic. A small amount of measurement noise significantly changes the performance of our algorithm unless the arrays of receivers and transmitters offer a directional diversity, see Fig. 6.

4.3 Ill-posedness in the limited-view setting

We undertake a numerical study to illustrate the ill-posedness of the linear system (6) in the case of limited-view data. Fig. 3 shows the distribution of eigenvalues of the matrix $\mathbf{C}^\top \mathbf{C}$ and $\mathbf{D}\mathbf{C}^\top \mathbf{C}\mathbf{D}$ at different values of γ with $N = 101$ and $K = 50$. In Fig. 4, we calculate the condition number of $\mathbf{C}^\top \mathbf{C}$ and \mathbf{L} (which is equal to that of $\mathbf{D}\mathbf{C}^\top \mathbf{C}\mathbf{D}$ by (31)) for different orders K . From these results, we see clearly the effect of the limited-view aspect. First, the tail of tiny eigenvalues in Fig. 3.(a) suggests that the matrix $\mathbf{C}^\top \mathbf{C}$ is numerically singular, despite the fact that \mathbf{C} is of maximal rank. Secondly, both $\mathbf{C}^\top \mathbf{C}$ and \mathbf{L} rapidly become extremely ill-conditioned as K increases, so the maximum resolving order of CGPTs is very limited. Furthermore, this limit is intrinsic to the angle of view and cannot be improved by increasing the number of source/receivers, see Fig. 4 (c) and (d).

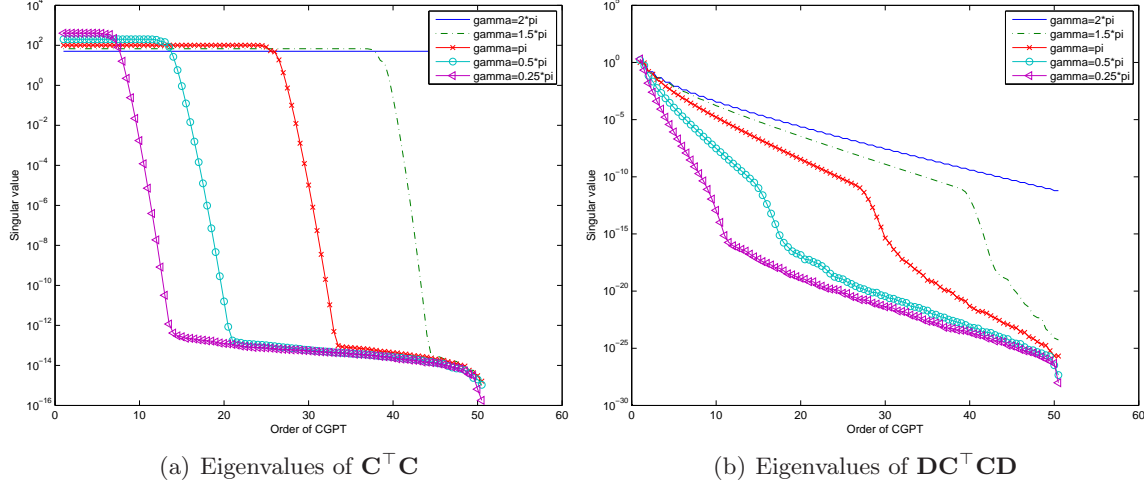
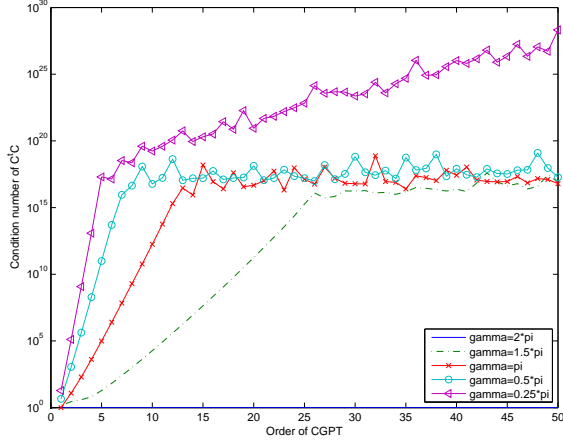
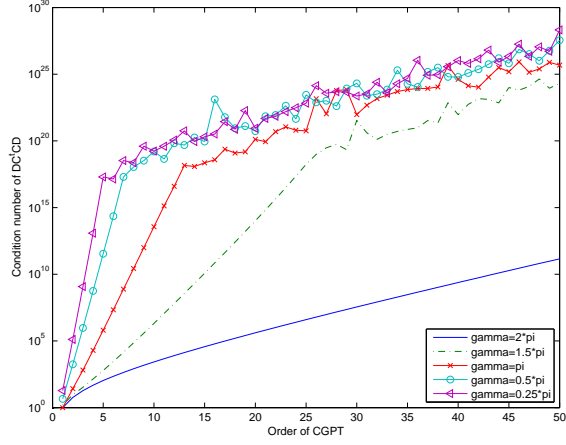


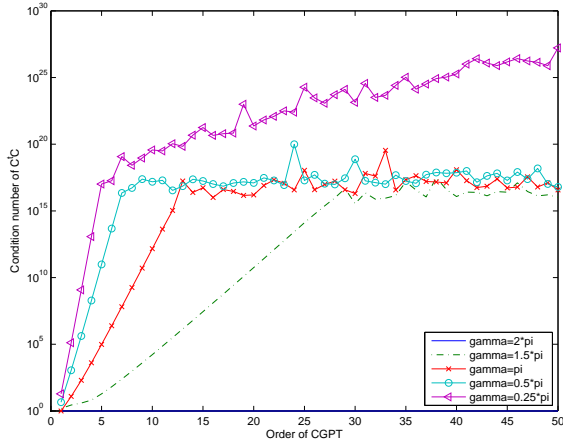
Figure 3: Distribution of eigenvalues (in log scale) of the matrix $\mathbf{C}^\top \mathbf{C}$ (a) and $\mathbf{D}\mathbf{C}^\top \mathbf{C}\mathbf{D}$ (b). $N = 101$ sources are equally spaced between $[0, \gamma)$ on a circle of radius $\rho = 1.2$, and $K = 50$. Each curve corresponds to a different value of γ . The matrix $\mathbf{C}^\top \mathbf{C}$ and $\mathbf{D}\mathbf{C}^\top \mathbf{C}\mathbf{D}$ are calculated from these parameters and their eigenvalues are sorted in decreasing order.



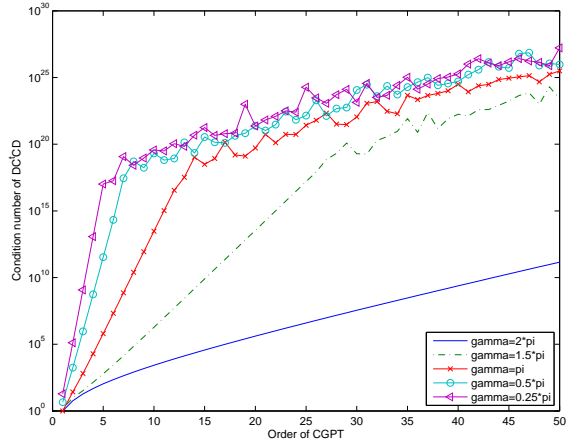
(a) Condition number of $\mathbf{C}^T \mathbf{C}$



(b) Condition number of \mathbf{L}



(c) Condition number of $\mathbf{C}^T \mathbf{C}$



(d) Condition number of \mathbf{L}

Figure 4: Condition numbers (in log scale) of the matrix $\mathbf{C}^T \mathbf{C}$ (a) and the operator \mathbf{L} (b) for different orders K between $[1, 50]$. As in Fig. 3, $N = 101$ sources are equally spaced between $[0, \gamma)$ on a circle of radius $\rho = 1.2$. Fig.(c) and (d) are the same experiment as Fig.(a) and (b) but with $N = 1001$.

4.4 Reconstruction of CGPTs

The analysis above suggests that the least-squares problem (7) is not adapted to the CGPT reconstruction in a limited-view setting. Actually, the truncation error or the noise of measurement will be amplified by the tiny singular values of \mathbf{L} , and yields extremely instable reconstruction of high-order CGPTs, *e.g.*, $K \geq 2$. Instead, we, in order to reconstruct CGPTs from the MSR data, use Thikhonov regularization and propose to solve

$$\min_{\mathbf{M}} \|\mathbf{L}(\mathbf{M}) - \mathbf{V}\|_F^2 + \mu \|\mathbf{M}\|_F^2, \quad (47)$$

with $\mu > 0$ a small regularization constant. It is well known that the effect of the regularization term is to truncate those singular values of \mathbf{L} smaller than μ , which consequently stabilizes the solution. The optimal choice of μ depends on the noise level, and here we determine it from the range $[10^{-6}, 10^{-1}]$ by comparing the solution of (47) with the true CGPTs.

Here we reconstruct the CGPTs of an ellipse with the parameter $N = 101, K = 50$, and γ varying between 0 and 2π . The major and minor axis of the ellipse are 1 and 0.5 respectively. In Fig. 5 we show the error of the first 2 order CGPTs reconstructed through (47) and (7) at three different noise levels. It can be seen that, for small γ , the error obtained by (47) is substantially smaller.

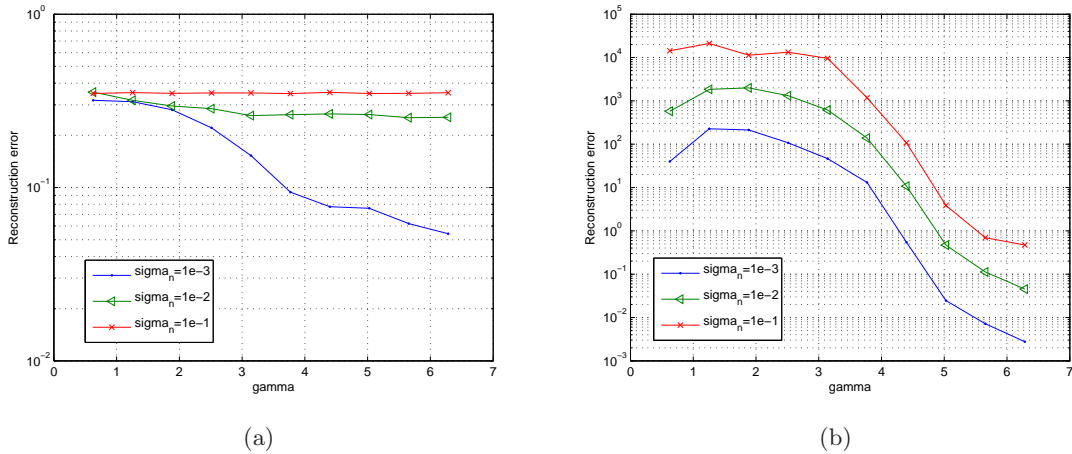


Figure 5: Error of reconstructed CGPT of an ellipse compared with true CGPT values at different noise levels. We solve (47) and (7) with $N = 101, K = 50$, and compare the first two orders with the true CGPT. The x -axis is the angle of view γ . Fig.(a): results of (47), Fig.(b): results of (7).

4.5 Tracking in the limited-view setting

The performance of the tracking algorithm can also be affected by the limited angle of view. We repeat the experiment of subsection 3.3 with $\delta = 10, \gamma = \pi$, and the same initial guess. In the first configuration, $N = 21$ sources/receivers are equally distributed between $[0, \gamma)$, see Fig. 6 (a). The results of tracking by EKF presented in Fig. 7 (a), (c)

and (e) show large deviations in the estimation of position, and a totally wrong estimation of orientation. In the second configuration, we divide the sources/receivers into 5 groups placed in a nonuniform way on $[0, 2\pi)$, and each group covers only an angle range of 0.2π , see Fig. 6 (b). Although the total angular coverages are the same in both configurations, the second one gives much better tracking results, as shown in Fig. 7 (b), (d) and (f). These results clearly demonstrates the importance of a large angle of view (or a directional diversity) for the tracking problem.

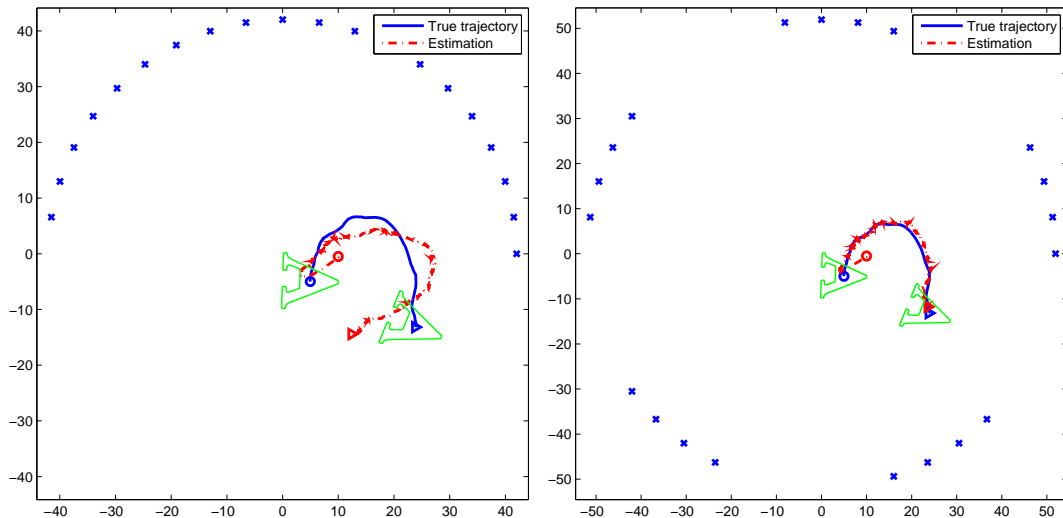


Figure 6: Same experiment as in Fig. 1, with a limited angle of view $\gamma = \pi$. In Fig.(a) sources/receivers are equally distributed between $[0, \gamma)$, while in Fig.(b) they are divided into 5 groups.

5 Conclusion

In this paper we have provided a location and orientation tracking of a mobile target from MSR measurements in the full- and limited-view settings. Our algorithm is based on the concept of GPTs. In the limited-view case, the effect of noise is severe on the tracking. However, if the arrays of receivers and transmitters offer a good directional diversity, then satisfactory results can be obtained. It would be interesting to generalize our algorithms for tracking multiple targets. As a first step, a matching pursuit algorithm [21] would be appropriate for recognizing the targets. This will be the subject of a forthcoming work.

A Kalman Filter

The KF is a recursive method that uses a stream of noisy observations to produce an optimal estimator of the underlying system state [20]. Consider the following time-discrete

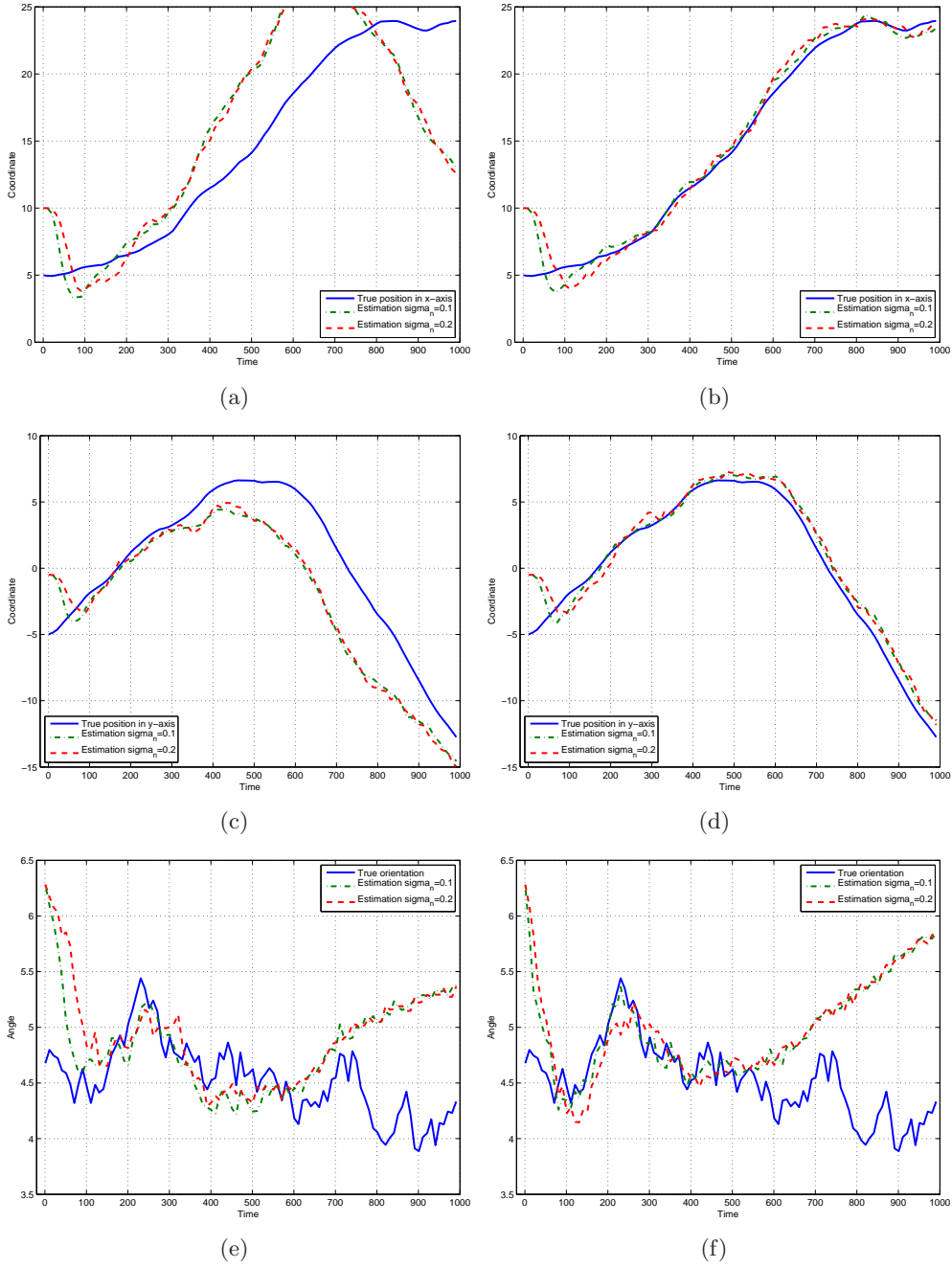


Figure 7: Results of tracking using the configuration of Fig. 6 at different noise levels. First row: coordinate in x -axis. Second row: coordinate in y -axis. Last row: orientation. First and second column correspond to the configuration in Fig. 6 (a) and (b), respectively.

dynamical system ($t \geq 1$):

$$X_t = F_t X_{t-1} + W_t, \quad (48)$$

$$Y_t = H_t X_t + V_t. \quad (49)$$

where

- X_t is the vector of *system state*;
- Y_t is the vector of *observation*;
- F_t is the state transition matrix which is applied to the previous state X_{t-1} ;
- H_t is the observation matrix which yields the (noise free) observation from a system state X_t ;
- $W_t \sim \mathcal{N}(0, Q_t)$ is the process noise and $V_t \sim \mathcal{N}(0, R_t)$ is the observation noise, with respectively Q_t and R_t the covariance matrix. These two noises are independent between them, further, W_t of different time instant are also mutually independent (the same for V_t).

Suppose that X_0 is Gaussian. Then it follows that the process $(X_t, Y_t)_{t \geq 0}$ is Gaussian. The objective is to estimate the system state X_t from the accumulated observations $Y_{1:t} := [Y_1 \dots Y_t]$.

The optimal estimator (in the least-squares sense) of the system state X_t given the observations $Y_{1:t}$ is the conditional expectation

$$\hat{x}_{t|t} = \mathbb{E}[X_t | Y_{1:t}]. \quad (50)$$

Since the joint vector $(X_t, Y_{1:t})$ is Gaussian, the conditional expectation $\hat{x}_{t|t}$ is a linear combination of $Y_{1:t}$, which can be written in terms of $\hat{x}_{t-1|t-1}$ and Y_t only. The purpose of the KF is to calculate $\hat{x}_{t|t}$ from $\hat{x}_{t-1|t-1}$ and Y_t .

We summarize the algorithm in the following.

Initialization:

$$\hat{x}_{0|0} = \mathbb{E}[X_0], \quad P_{0|0} = \text{cov}(X_0). \quad (51)$$

Prediction:

$$\hat{x}_{t|t-1} = F_t \hat{x}_{t-1|t-1}, \quad (52)$$

$$\tilde{Y}_t = Y_t - H_t \hat{x}_{t|t-1}, \quad (53)$$

$$P_{t|t-1} = F_t P_{t-1|t-1} F_t^T + Q_t. \quad (54)$$

Update:

$$S_t = H_t P_{t|t-1} H_t^T + R_t, \quad (55)$$

$$K_t = P_{t|t-1} H_t^T S_t^{-1}, \quad (56)$$

$$\hat{x}_{t|t} = \hat{x}_{t|t-1} + K_t \tilde{Y}_t, \quad (57)$$

$$P_{t|t} = (I - K_t H_t) P_{t-1|t-1}. \quad (58)$$

To apply the KF algorithm the covariance matrices Q_t, R_t must be known.

B Extended Kalman Filter

Consider now a nonlinear dynamical system:

$$X_t = f_t(X_{t-1}, W_t), \quad (59)$$

$$Y_t = h_t(X_t, V_t), \quad (60)$$

where X_t, Y_t, W_t, V_t are the same as in the KF, while the functions f_t, h_t are nonlinear and differentiable. Nothing can be said in general on the conditional distribution $X_t|Y_{1:t}$ due to the nonlinearity. The EKF calculates an approximation of the conditional expectation (50) by an appropriate linearization of the state transition and observation models, which makes the general scheme of KF still applicable [26]. However, the resulting algorithm is no more optimal in the least-squares sense due to the approximation.

Let $F_X = \partial_X f(\hat{x}_{t-1|t-1}, 0)$, $F_W = \partial_W f(\hat{x}_{t-1|t-1}, 0)$, the partial derivatives of f (with respect to the system state and the process noise) evaluated at $(\hat{x}_{t-1|t-1}, 0)$, and let $H_X = \partial_X h(\hat{x}_{t|t-1}, 0)$, $H_V = \partial_V h(\hat{x}_{t|t-1}, 0)$ be the partial derivatives of h (with respect to the system state and the observation noise) evaluated at $(\hat{x}_{t|t-1}, 0)$. The EKF algorithm is summarized below.

Initialization:

$$\hat{x}_{0|0} = \mathbb{E}[X_0], \quad P_{0|0} = \text{cov}(X_0). \quad (61)$$

Prediction:

$$\hat{x}_{t|t-1} = f(\hat{x}_{t-1|t-1}, 0), \quad (62)$$

$$\tilde{Y}_t = Y_t - h(\hat{x}_{t|t-1}, 0), \quad (63)$$

$$P_{t|t-1} = F_X P_{t-1|t-1} F_X^T + F_W Q_t F_W^T. \quad (64)$$

Update:

$$S_t = H_X P_{t|t-1} H_X^T + H_V R_t H_V^T, \quad (65)$$

$$K_t = P_{t|t-1} H_X^T S_t^{-1}, \quad (66)$$

$$\hat{x}_{t|t} = \hat{x}_{t|t-1} + K_t \tilde{Y}_t, \quad (67)$$

$$P_{t|t} = (I - K_t H_X) P_{t-1|t-1}. \quad (68)$$

References

- [1] H. Ammari, T. Boulier, and J. Garnier, Modeling active electrolocation in weakly electric fish, Arxiv preprint arXiv:1203.0938, 2012. To appear in SIAM J. Imag. Sci., 2012. [2](#)
- [2] H. Ammari, T. Boulier, J. Garnier, W. Jing, H. Kang, and H. Wang, Target identification using dictionary matching of generalized polarization tensors, Arxiv preprint arXiv:1204.3035, 2012. [2](#), [3](#), [5](#), [6](#), [7](#), [10](#)
- [3] H. Ammari, J. Garnier, H. Kang, M. Lim, and S. Yu, Generalized polarization tensors for shape description, submitted, 2011. [1](#)

- [4] H. Ammari and H. Kang, *Reconstruction of small inhomogeneities from boundary measurements*, Vol. 1846, Lecture Notes in Mathematics, Springer-Verlag, Berlin, 2004. [1](#), [2](#), [3](#)
- [5] H. Ammari and H. Kang, *Polarization and moment tensors: with applications to inverse problems and effective medium theory*, Vol. 162, Springer-Verlag, 2007. [2](#)
- [6] H. Ammari and H. Kang, High-order terms in the asymptotic expansions of the steady-state voltage potentials in the presence of conductivity inhomogeneities of small diameter, *SIAM J. Math. Anal.*, 34 (2003), 1152–1166. [1](#), [2](#), [3](#)
- [7] H. Ammari and H. Kang, Properties of generalized polarization tensors, *SIAM Multi-scale Model. Simul.*, 1 (2003), 335–348. [1](#)
- [8] H. Ammari, H. Kang, M. Lim, and H. Lee, Enhancement of near cloaking using generalized polarization tensors vanishing structures. Part I: The conductivity problem, *Comm. Math. Phys.*, to appear. [1](#), [2](#), [3](#)
- [9] H. Ammari, H. Kang, M. Lim, and H. Zribi, The generalized polarization tensors for resolved imaging. Part I: Shape reconstruction of a conductivity inclusion, *Math. Comp.*, 81 (2012), 367–386. [1](#)
- [10] H. Ammari, H. Kang, and K. Touibi, Boundary layer techniques for deriving the effective properties of composite materials, *Asymp. Anal.*, 41 (2005), 119–140. [1](#)
- [11] Y. Capdeboscq, A. B. Karrman, and J.-C. Nédélec, Numerical computation of approximate generalized polarization tensors, *Appl. Anal.*, to appear. [2](#)
- [12] D.J. Cedio-Fengya, S. Moskow, and M.S. Vogelius, Identification of conductivity imperfections of small diameter by boundary measurements: Continuous dependence and computational reconstruction, *Inverse Problems*, 14 (1998), 553–595. [2](#)
- [13] M. Cheney and B. Borden, Imaging moving targets from scattered waves, *Inverse Problems*, 24 (2008), 035005. [2](#)
- [14] D. Clark, I.T. Ruiz, Y. Petillot, and J. Bell, Particle PHD filter multiple target tracking in sonar images, *IEEE Trans. Aerospace Electr. Sys.*, 43 (2007), 409–416. [2](#)
- [15] G. Dassios and R. Kleinman, *Low frequency scattering*, Oxford Mathematical Monographs, Oxford University Press, New York, 2000. [1](#)
- [16] D. Daviesy, P. Palmery, and M. Mirmehdi, Detection and tracking of very small low contrast objects, *British Machine Vision Conference*, 1998, 599–608. [2](#)
- [17] A. Friedman and M.S. Vogelius, Identification of small inhomogeneities of extreme conductivity by boundary measurements: a theorem on continuous dependence, *Arch. Rat. Mech. Anal.*, 105 (1989), 299–326. [2](#)
- [18] C.D. Haworth, Y. De Saint-Pern, D. Clark, E. Trucco, and Y.R. Petillot, Detection and tracking of multiple metallic objects in millimetre-wave images, *Inter. J. Comput. Vision*, 71 (2007), 183–196. [2](#)

- [19] J.S. Jaffe, Target localization for a three-dimensional multibeam sonar imaging system, *J. Acoust. Soc. Am.*, 105 (1999), 3168–3175. [2](#)
- [20] R.E. Kalman, A new approach to linear filtering and prediction problems, *Transaction of the ASME–Journal of basic Engineering* 82 (1960), 35–45. [18](#)
- [21] S. Mallat, *A Wavelet Tour of Signal Processing*, Academic Press, San Diego, 1998. [18](#)
- [22] E. Margolis and Y.C. Eldar, Nonuniform sampling of periodic bandlimited signals, *IEEE Trans. Sig. Process.*, 56 (2008), 2728–2745. [14](#)
- [23] G.W. Milton, *The Theory of Composites*, Cambridge Monographs on Applied and Computational Mathematics, Cambridge University Press, 2001. [1](#)
- [24] G. Pólya and G. Szegő, *Isoperimetric Inequalities in Mathematical Physics*, Annals of Mathematical Studies, Number 27, Princeton University Press, Princeton, NJ, 1951. [1](#)
- [25] L. Wang, M. Cheney, and B. Borden, Multistatic radar imaging of moving targets, *IEEE Radar Conference*, 391–396. [2](#)
- [26] G. Welch and G. Bishop, An introduction to the Kalman filter, Technical Report 95-041, University of North Carolina at Chapel Hill, 2001 & SIGGRAPH 2001, Los Angeles, CA, August 12–17, ACM. [2](#), [21](#)
- [27] A. Zygmund, *Trigonometric series*, Cambridge Univ Press, Cambridge, 1988. [14](#)

